On the behaviour of nanoparticles in oil-in-water emulsions with different surfactants

Johann Lacava,[†] Ahmed-Amine Ouali,[†] Brice Raillard,[‡] and Tobias Kraus[*,†]

Structure Formation Group,

INM — Leibniz-Institute for New Materials,

Campus D2 2, 66123 Saarbrücken, Germany, and

E-mail: tobias.kraus@inm-gmbh.de

Phone: +49-681-9300-359. Fax: +49-681-9300-279

Abstract

The distribution of narrowly dispersed gold nanoparticles in hexane-in-water emulsions was studied for different surfactants. Good surfactants such as SDS and Triton X-100 block the interface and confine particles in the droplet. Other surfactants (Tween 85, Span 20) form synergistic mixtures with the nanoparticles at the interfaces that lower the surface more than any component. Supraparticles with fully defined particle distribution only form for surfactants that block the interface. Other surfactants promote the formation of fcc agglomerates. Nanoparticles in emulsions behave markedly different from microparticles — their structure formation is governed by free energy minimization, while microparticles are dominated by kinetics.

[*]To whom correspondence should be addressed

[†]INM — Leibniz-Institute for New Materials, Structure Formation Group, Campus D2 2, 66123 Saarbrücken, Germany

[‡]Chair of functional Materials, Saarland University, Campus D3 3, 66123 Saarbrücken, Germany

Introduction

Colloidal nanoparticles have useful magnetic, electronic and optical properties. They are exploited in particle-polymer nanocomposites that inherit properties from single particles or their collective behavior. Engineered combinations of nanoparticles into defined, larger structures can extend this principle towards more complex functionality. "Particle clusters" or "supraparticles" are combinations of nanoparticles in the form of colloids that can be embedded in hybrid materials using existing methods.[1–3]

Emulsion droplets are convenient templates to confine and combine particles into supraparticles by evaporating the disperse solvent.[4–8] Manoharan, Elsesser and Pine found that when colloidal microspheres adsorb onto the liquid-liquid interface of emulsions, removing fluid from the droplets leads to predictable packing of the spheres.[9] We showed that nanoparticles that are confined inside emulsion droplets can form clusters with predictable geometries by free energy minimization.[10]

Particle-laden emulsions are commonly used for the encapsulation of (micro- and nanoscale) particles in pharmaceutical formulations, cosmetics and in the food industry. This yields capsules with less structural control. Recent strategies for drug release, functional foods or modern cosmetics indicate a trend to complex, designed structures in these fields, too.[11–13]

Structure formation in particle-containing emulsions strongly depends on the interactions between nanoparticles and the liquid-liquid interface. Both surfactants and nanoparticles can adsorb at the liquid-liquid-interface. After adsorption, surfactants and particles alone[14] and their combinations[15,16] can stabilize emulsions. Depending on which components segregate to the liquid-liquid interface, structure formation follows different routes during the evaporation of the dispersed solvent.

Previous studies of nanoparticle-containing emulsions focused mainly on the effects of particles and surfactants on surface tension and emulsion stability. Ma et al. studied the assembly of anionic and cationic surfactants and negatively charged silica nanoparticles at the trichloroethene-water interface. Silica nanoparticles increased the efficiency of the anionic surfactant, Sodium dodecyl sulfate (SDS), but provide no synergistic effect when combined with non-ionic surfac-

tants. The authors concluded that repulsive interactions between SDS and nanoparticles promote surfactant adsorption at the interfaces.[17] Whitby et al. studied the addition of SDS to dodecane-in-water Pickering emulsion stabilized by silica nanoparticles.[18] At SDS concentrations above the critical micelle concentration (cmc), the rate of flocculation and creaming were enhanced. Some years later, Vashisth et al. used confocal fluorescence microscopy and cryogenic scanning electron microscopy to show that adding SDS to Whitby's emulsions leads to the displacements of nanoparticles from the interface at surfactant concentration above the cmc. At surfactant concentrations below the cmc, mixtures of particles and surfactant populated the liquid-liquid interfaces.[19]

Recently, surprising properties of mixtures of oleylamine with silica nanoparticles in oil-in-water emulsions were observed. The interfacial tension of the oil-in-water emulsion increased with the concentration of silica nanoparticle in the oil phase.[20] Eskandar et al. suggested that the attraction between oppositely charged nanoparticles and surfactants results in the adsorption of surfactant on the nanoparticles' surfaces and reduces the surfactant density at the oil-water interface.

In this report, we use monodispersed gold nanoparticles (AuNP) with oleophilic surfaces to probe the structure formation of supraparticles in oil-in-water emulsions containing the anionic surfactant sodium dodecyl sulfate "SDS" or one of the two non-ionic surfactants sorbitan monolaurate "Span 20" and polyethylene glycol sorbitan trioleate "Tween 85". Tween 85 has a molecular mass that is more than 4 times that of Span 20. The chosen surfactants span a wide range of HLB indices (Table 1).

The AuNP are optically active and strong x-ray scatterers, which makes in-situ analysis straightforward. We slowly evaporate the oil phase of particle-containing emulsions and observe conformational changes as surfactant and particle concentrations increase. We compare the behavior of macroscopic oil-water interfaces in the presence of the same surfactants and nanoparticles. We draw conclusions on the relationship between interfacial tensions, adsorption of moieties at the oil-water-interface, and the morphology of the particle superstructures formed.

Experimental Section

Materials

All chemicals were obtained from the denoted sources and used without further purification. Different commercially available surfactants were studied: Sodium dodecyl sulfate (SDS), Sorbitan monolaurate (Span 20), and Polyethylene glycol sorbitan trioleate (Tween 85) were purchased from Sigma-Aldrich. Table 1 introduces some of their properties as provided by the manufacturers and the references mentioned in Table 1.

Table 1: Some properties of surfactants used for the preparation of emulsions

	Type	HLB	Molecular weight [g/mol]	CMC [mmol]	Density [g/mL]
Tween 85	non-ionic	11	1838.5	0.00029[21]	1.028
Span 20	non-ionic	8.6	346.47	0.021[22]	1.032
SDS	anionic	–	289	8.2[23]	1.01

AuNP with core diameters of 6 nm were synthesized using a route adapted from Zheng et al.[24] They were formed in a one-pot reduction of a gold source by an amine-borane complex in the presence of an alkyl thiol. Chlorotriphenylphosphine gold (ABCR, minimum purity 98%) was mixed with dodecanethiol (Fluka, 98%) in benzene (Riedel-de-Hahn, 99.5%) to form a clear solution to which the tert-butylamine-borane complex (Fluka, 97%) was subsequently added. The mixture was heated to 55 °C for 2 h during which the solution turned into a dark purple color indicating nanoparticle formation. After the reduction reaction the AuNP suspension was cooled to room temperature, the particles were precipitated by the addition of ethanol, washed by centrifugation and subsequently resuspended in toluene. For cluster formation experiments, the particles were finally resuspended in n-hexane (Sigma-Aldrich, 98.5%).

Preparation of oil-in-water emulsions

Nanoparticle-containing emulsions were prepared by emulsification of a nanoparticle dispersion in water containing different surfactants. Efficient emulsification was achieved by mechanical shearing. In a typical experiment, AuNP dispersions in hexane were mixed with ultrapure water (Milli-Q water purification system type ELIX 20, Millipore Corp., USA) and an aqueous solution of surfactant (see Table2). The surfactant concentration was adjusted to be above cmc. Exact concentrations are given in table 2.

Table 2: Emulsion characteristics

	Tween 85	Span 20	SDS
Volume water [mL]	16	16	12.32
Volume gold suspension [μL]	320	320	320
Volume surfactant [μL]	320	320	4000
Concentration of surfactant in emulsion [mmol]	0.11	0.57	8.4

The mixtures were emulsified using an Ultra-Turrax benchtop homogenizer (Ultra-Turrax Typ T-25, IKA-Werke GmbH, Staufen, Germany) at $20,500$ rpm during 30 min

The dispersed solvent was removed from the emulsion droplets by evaporation. In the simplest case, the oil phase was left to evaporate at room temperature and ambient pressure during at least 12 h. For the synchrotron SAXS study, evaporation was enhanced using a nitrogen stream. A sealed vessel containing the emulsion was submerged into a thermostated bath and kept at 298 K. The vessel was connected to a nitrogen stream that bubbled through the emulsion to permit evaporation of the dispersed solvent in only 4 h.

Surface plasmon spectroscopy

UV-Vis spectrometry was performed using a Cary 5000 photospectrometer (Varian Inc., USA) that recorded spectra in the wavelength range from 200 nm to 800 nm. Approximately 1 mL of the

respective sample was measured using a quartz cuvette with a beam path of 1 cm. The spectrum of the background (water) was subtracted from the samples' UV-Vis spectra.

We assume identical droplets and use the Maxwell-Garnett effective medium approximation (EMT) to calculate an effective dielectric constant ε_{eff} of a droplet that contains the solvent with a dielectric constant ε_m and particles with a dielectric constant ε^∞:[25,26]

$$\varepsilon_{eff} = \varepsilon_m \left(1 + \frac{3\phi\beta}{1-\phi\beta}\right) \text{, with } \beta = \frac{\varepsilon^\infty - \varepsilon_m}{\varepsilon^\infty + 2\varepsilon_m} \tag{1}$$

where ϕ is the volume fraction of particles, ε_m is the dielectric constant of the medium and ε^∞ is the dielectric constant of the metals depending on interband transitions. For gold, we use $\varepsilon^\infty = 11$.[27,28] The increasing particle concentration in the shrinking droplets changes the dielectric environment during evaporation and causes the surface plasmon shift. The surface plasmon resonance (SPR) frequency of particles in a droplet with a volume fraction of particles ϕ and an effective dielectric constant of ε_{eff} is then:

$$\begin{aligned} \lambda_{spr} &= 2\pi c \sqrt{\frac{m_e \varepsilon_0}{Ne^2}(\varepsilon^\infty + 2\varepsilon_{eff})} \\ &= 2\pi c \sqrt{\frac{m_e \varepsilon_0}{Ne^2}\left(\varepsilon^\infty + 2\varepsilon_m\left(1 + \frac{3\phi\beta}{1-\phi\beta}\right)\right)}. \end{aligned} \tag{2}$$

with N the concentration of free electrons in the metal, m_e the effective mass of electrons and the vacuum permittivity ε_0.

It was previously determined that the electrons density of gold nanoparticles is 5.9×10^{28} /m^3.[29]

Transmission electron microscopy

Morphological and structural characterization were carried out with a CM 200 electron microscope (Philips, Netherlands) operating at 200 keV. Samples were prepared by placing a drop of the supraparticle-containing dispersion on the surface of a carbon-coated copper grid and allowing the

grid to dry in air. To determine the mean size of the gold cores of the particles and the interparticle distance between agglomerated nanoparticles, several dozens of particles were evaluated using the ImageJ analysis software(available for free download from the NIH).

Tensiometry

Interfacial tension measurements were carried out on a DSA 100 pendant drop tensiometer (Krüss GmbH, Germany) which we used as a drop shape analyzer. Measurements were performed at an ambient temperature of 295 K $\pm$ 1 K. Drop images were acquired by a black and white high-speed camera and analyzed using the DSA3 software supplied by the manufacturer (Krüss GmbH, Germany). To measure the oil-water interfacial tension, the continuous phase was filled into a quartz glass cuvette. The dispersed phase was filled into a glass syringe which was connected to a J-shaped needle that protruded into the cuvette. The interfacial tension values were obtained by fitting the profile of the pendant drop to its theoretical shape using the DSA3 software.The arithmetic mean and the standard deviation of at least three measurements were used as interfacial tension values.

Pendant droplet analysis requires the drop to be significantly deformed by gravity. The volume of the drops was chosen such that they were deformed by gravity, just before the point of break-off from the needle tip. Since the shape of the drop depends on the interfacial tension of the system, different volumes (between 1 µL and 20 µL) were chosen depending on the system studied.

The concentration of gold in hexane was 0.38 mg/mL. All surfactants were at concentrations considerably above cmc, approximately 9 mmol of SDS in water, approximately 1 mmol of Tween 85 in water and approximately 1 mmol of Span 20 in water. The drops assumed their equilibrium shapes after 1 min; repeated measurements were peformed during 5 min until a plateau was reached that we report as the equilibrium interfacial tension.

Dynamic light scattering

Dynamic light scattering (DLS) was performed using a laser scattering goniometer (CGS-3, ALV GmbH, Germany) equipped with a 35 mW Helium-Neon laser emitting at a wavelength of 632.8 nm. The scattered light was collected at 90° scattering angle, split and detected by two avalanche photodiodes. A hardware correlator (ALV-7004, ALV GmbH, Germany) correlated the scattered intensity in real time and calculated the normalized intensity correlation function as a function of delay time. The sample was contained in a 1-cm-diameter glass cuvette inside a sample chamber filled with toluene. Its temperature was held at 293 K by a thermostated, circulating water bath (Phoenix II, Haake, Germany).

Small angle X-ray scattering

The volume fraction of the droplets in the emulsion is so low that synchrotron radiation becomes necessary for in-situ x-ray scattering experiments. Small-angle x-ray scattering (SAXS) experiments were carried out at the beam line ID02 of the European Synchrotron Radiation Facility (ESRF) in Grenoble, France. The experiments were repeated for two different sample-detector distances (10 m and 1 m) to cover a wide q range . The scattering vector q characterizes the momentum transfer, $q = 4\pi\lambda^{-1}\sin\theta$, with a wavelength of $\lambda = 0.1$ nm and the scattering angle 2θ between 0.009 and 6°.

During the evaporation of the particle-containing emulsion, 0.3 µL emulsion were removed every 10 min, introduced into a flow-through capillary cell (outside diameter approximately 2 mm, wall thickness approximately 0.01 mm) and characterized in a SAXS measurement. The procedure was repeated until the dispersed solvent had evaporated completely. Two different emulsions were analysed subsequently at the two sample-detector distances. We used the same cell during all experiments to enable reliable subtraction of the background. The two-dimensional scattering images were radially averaged, a water background was subtracted and the data was analyzed using ESRF's SAXSutilities software.[30]

Results

Three aspects of particle-containing hexane-in-water emulsions were analyzed: the effect of surfactants and particles on the surface tension of macroscopic hexane-water interfaces, the distribution of particles in emulsion droplets, and the changes in distribution and agglomeration of particles when the dispersed phase was evaporated.

Interfacial tension of macroscopic drops

Only particles and surfactants that adsorb at the oil-water interface can change its interfacial tension. Figure 1 (a) shows the hexane-water interfacial tension calculated from the shapes of macroscopic oil drops for different surfactant and nanoparticle contents. The presence of AuNP in hexane without any surfactant decreased the interfacial tension from 53 mN/m to 37 mN/m, consistent with results of Glaser et al.[31] and indicating that nanoparticles segregated to the interface.

We added surfactants to the aqueous phase at concentrations just above cmc (see Table 1). The additon of SDS in the absence of particles (hatched columns) reduced the interfacial tension to 11.8 mN/m, whereas the addition of Tween 85 and Span 20 only reduced the interfacial tension to 30.9 mN/m and 34 mN/m, respectively. The observed tensions are slightly above literature values measured using the ring method of de Nouy.[32,33] Such discrepancies have been reported earlier and discussed in depth by Yeung et al,[34] who suggested that the equilibrium partitioning of the surfactant depends on the surface-to-volume ratio of the fluid body analyzed.

The grey columns in figure 1 (a) show the interfacial tension for oil drops containing nanoparticles in surfactant solution. The particles did not change the tension of oil drops in SDS solution. For Tween 85 and Span 20, the interfacial tension decreased to 15.3 mN/m and 14.1 mN/m, respecively, values that are below both particle-containing hexane in water and pure hexane in the surfactant solutions.

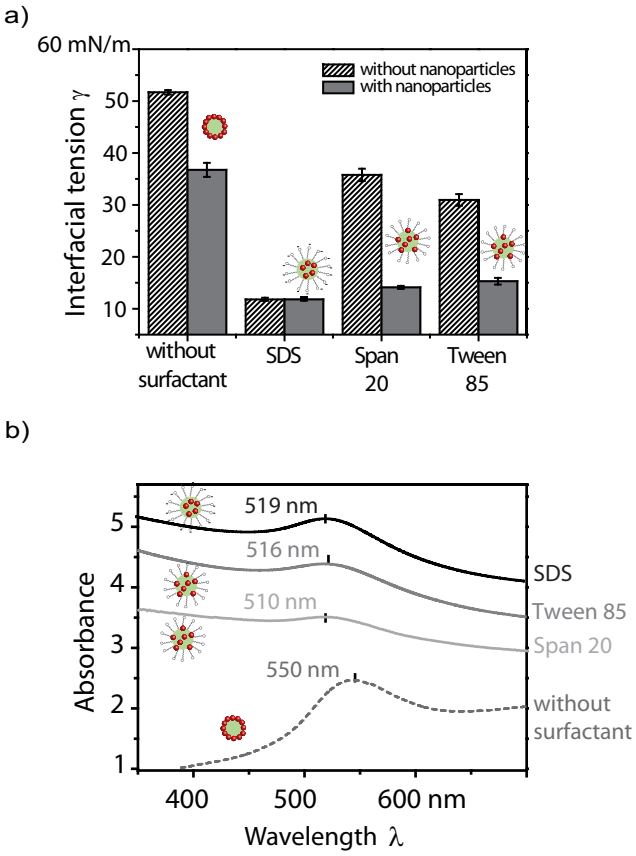

Figure 1: a) Equilibrium interfacial tensions of hexane-water interfaces with different surfactants and particles. All values were calculated from the shapes of macroscopic pendant drops. Surfactants were introduced into the continuous phase (water) at concentrations above the critical micelle concentration, AuNP were introduced into the dispersed phase (hexane). b) UV-Vis spectra of emulsions containig AuNP just after emulsification. Emulsions containing surfactants exhibited a surface plasmon resonance peak around 517 nm. The peak is shifted to higher wavelengths in the absance of surfactants.

Particle distribution in microscopic droplets

It is difficult to perform tensiometry on the microscopic droplets of an emulsion. Instead, we used surface plasmon spectroscopy to observe the migration of nanoparticles inside the droplets. The method indicates the close packing of nanoparticles that occurs when they densely populate the oil-water interface.

Figure 1 (b) shows the UV-Vis spectra of particle-containing emulsions for different surfactants. We evaluated the position of the surface plasmon resonance (SPR) just after emulsification. In the absence of any surfactant, the original peak position of 520 nm drastically red-shifted to 550 nm, indicating a localized concentration increase of the AuNP that we interpret as migration to the interface. In the presence of SDS, no SPR shift was observed, consistent with nanoparticles that remain dispersed in the bulk. Surprisingly, emulsions containing Tween 85 or Span 20 did not exhibit any shift of the SPR signal despite of their effect on macroscopic interfacial tension.

Evaporation of oil from microscopic droplets

The nanoparticle concentration in the oil phase is much lower than the surfactant concentration in the aqueous phase. It is interesting to know whether the emulsion structure changes for higher concentrations. We increased the particle concentration by slowly evaporating the oil phase while constantly monitoring the SPR peak. Concurrent DLS measurements were performed to determine the evolution of the droplet size during the evaporation. The evaporation rate was kept low to create quasi-static, near-equilibrium situations.

Figure 2 shows the SPR evolution during the evaporation of emulsions containing different surfactants. Each point in the graphs indicates the mean and standard deviation of the droplet size and surface plasmon peak shift observed after the same evaporation time in three separate experiments. The insets show the SPR peaks recorded during the evaporation process. Larger droplets that are present at the beginning of the experiment scatter the light more strongly than the partially evaporated droplets at later stages. To the naked eye, the samples' appearance change from turbid to clear during evaporation. This explains the increasing overall transmission (see insets). The SPR

peak becomes clearly visible after around 120 min, when the background scattering has decreased sufficiently.

For emulsions stabilized by SDS or Tween 85 (Figure 2 (a) and (b)), the average droplet size decreased continuously. Concurrently, the SPR peak shifted, with a marked rate increase towards the end of the evaporation process. We previously studied the behavior of AuNP in emulsions stabilized by Triton X-100 and found very similar evolutions of droplet size and SPR peaks.[10] They coincide with values theoretically predicted using the effective medium approximation assuming homogeneously distributed particles (see section Materials and Methods). The calculated shifts are indicated by the continuous lines in Figure 2 (a) and (b).

For emulsions stabilized by Span 20 (Figure 2 (c)), the average droplet size increased during the first 180 min to then decrease until the end of the evaporation. The SPR shift remained fixed while the droplet size increased. The final shift was comparable to that observed for other surfactants.

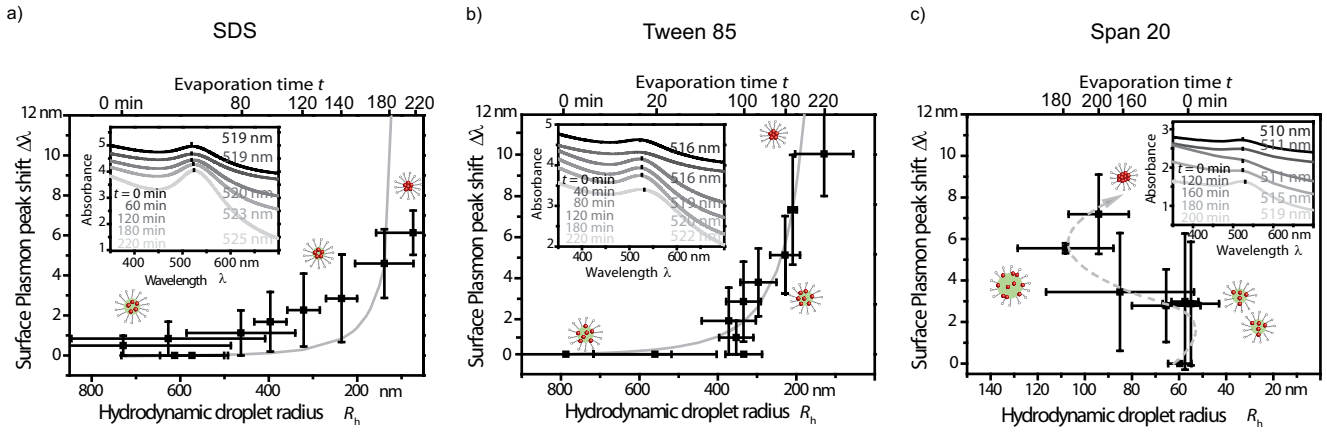

Figure 2: Analysis of the cluster formation mechanism by UV-Vis spectroscopy. Samples were taken from evaporating emulsions containing (a) SDS, (b) Tween 85 and (c) Span 20 and analyzed for the position of the particles' surface plasmon peak. The continuous lines in graphs (a) and (b) indicate the shift predicted by an EMT model for homogeneously distributed particles. For samples containing SDS and Tween 85, the SPR peak markedly shifted towards the end of the evaporation process when the droplet size decreased rapidly. For samples containg Span 20, the droplet radii increased initally (with fixed SPR) and then decreased (with increasing SPR shift).

While SPR spectroscopy only indicates local concentration changes, synchrotron small-angle x-ray scattering (SAXS) provides details on their distribution. Particle-containing emulsions were

evaporated at the synchrotron and samples were taken for scattering measurements at fixed intervals. References were obtained from nanoparticles in pure hexane. The SAXS Utilities software of ESRF was used to fit the reference data and determined radii of $2.95\,\mathrm{nm} \pm 0.10\,\mathrm{nm}$.

Figure 3 (a) shows the evolution of scattering during the evaporation process for the three surfactants. All samples exhibited strong oscillations in the high q-region ($q > 0.5\,\mathrm{nm}^{-1}$) that indicate nanoparticles with a narrow size distribution. In the low q region ($q < 0.1\,\mathrm{nm}^{-1}$), where larger structures dominate, no oscillations were visible.

We calculated a structure factor $S(q)$ from the radially integrated scattering intensity $I(q)$ using

$$S(q) = \frac{I(q)}{F(q)} \tag{3}$$

with a theoretical form factor $F(q)$ calculated from the particle geometry obtained in reference measurements. Figures 3 (d)–(f) show the evolution of the structure factor of three emulsions during the evaporation process.

Structure of nanoparticle clusters

After all oil has evaporated, particle agglomerates remain dispersed due to the stabilizing effect of the surfactant. These agglomerates can be internally ordered ("supraparticles" or "clusters"[10]) or disordered. Figure 4 shows transmission electron micrographs (TEM) of agglomerates formed in emulsions containing differents surfactants. Emulsions containing SDS yielded a large fraction of supraparticles. A part of them was structurally similar to clusters formed from particles interacting with Lennard-Jones potentials.[10] Tween 85 and Span 20 (figure 4 (c) and (d)) yielded a large fraction of isolated particles and irregularly shaped agglomerates. Small numbers of supraparticles were present, too, but they were composed of crystalline "grains" having fcc structure rather than having Lennard-Jones-like features.

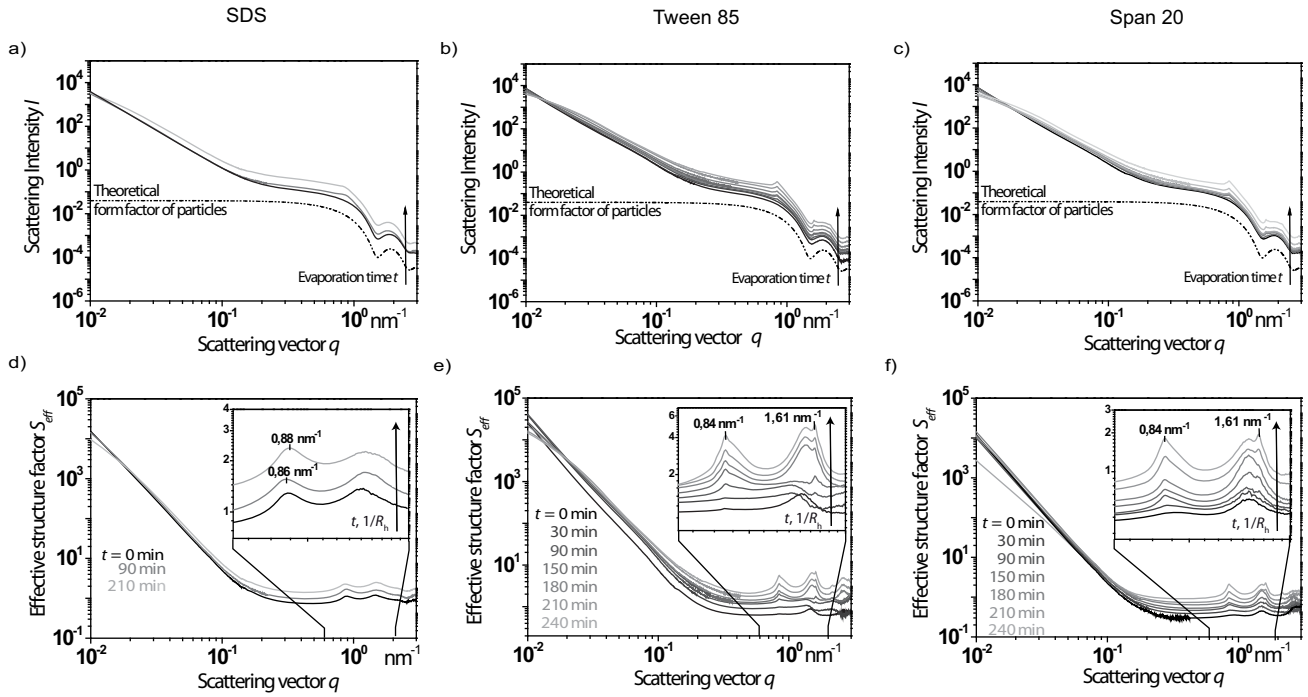

Figure 3: Analysis of the cluster formation mechanism by Small-angle X-ray scattering. Samples were taken from the evaporating emulsion and analyzed. The evolution of the scattering intensity for samples containing SDS (a) is similar to that reported for Triton X-100-containing emulsions, where supraparticle form.[10] A characteristic peak in the structure factor (d) emerges and shifts to larger values until evaporation has completed. It indicates the formation of increasingly dense clusters. Samples containing Tween 85 (b) or Span 20 (c) deviate from SDS and Triton X-100. Two peaks in the structure factor (e and f) occur early and remain and constant q during the evaporation process.

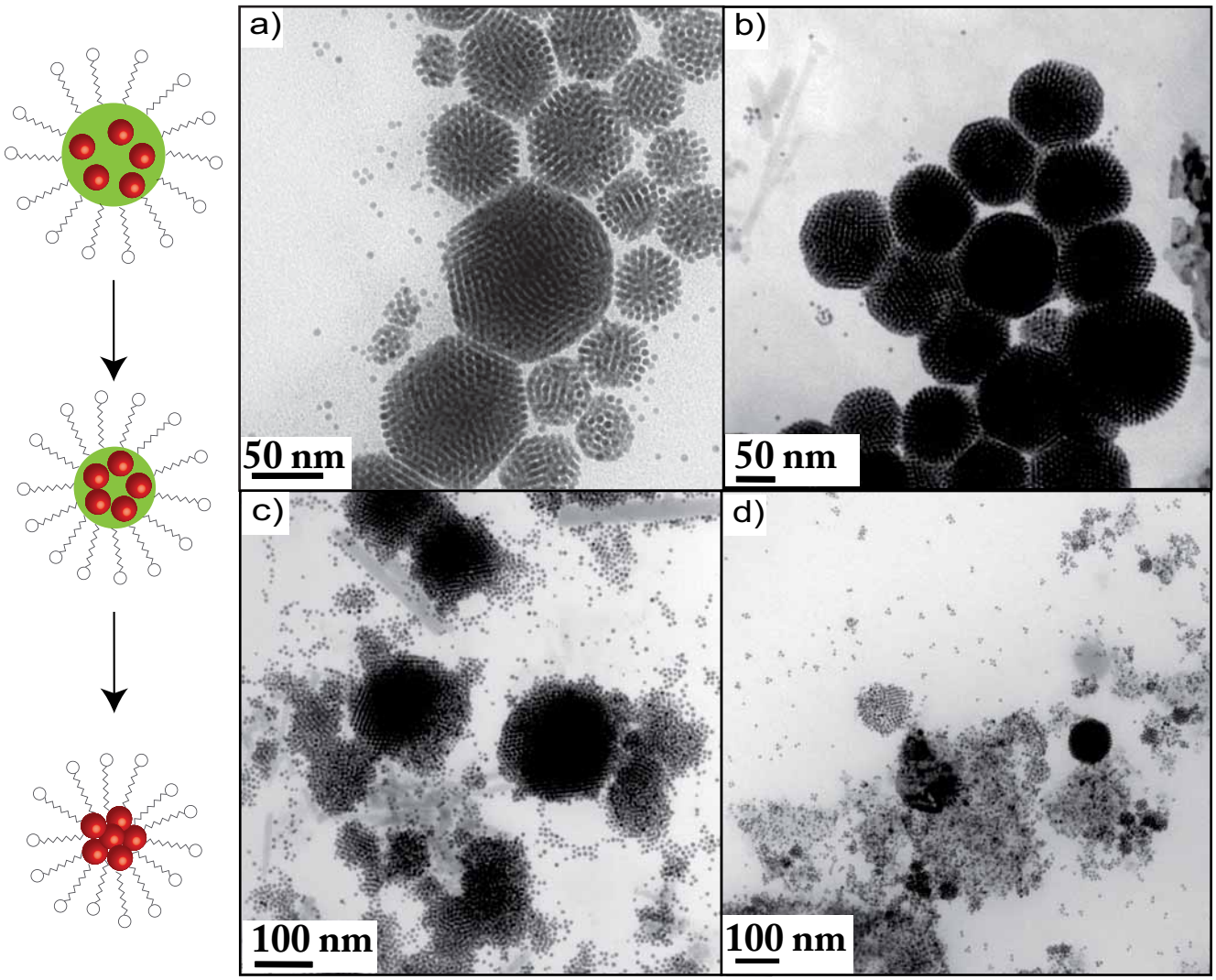

Figure 4: Transmission electron micrographs of nanoparticle agglomerates formed in emulsion droplets. Supraparticles with Lennard-Jones-cluster geometries form in emulsions stabilized (a) with Triton X-100 (as reported previously in[10]) and (b) SDS. Emulsions stabilized by Tween 85 (c) and Span 20 (d) yield disordered agglomerates and smaller amounts of agglomerates with regions that exhibit fcc packing.

Discussion

Both the macroscopic surface tension of hexane-water interfaces and the microscopic distribution of particles in emulsion droplets depended on the surfactant-particle combination. We believe that free energy minimization leads to a competition between particles and surfactants for adsorption sites at the oil-water interface. In the absence of surfactant, particles populate the interface. The most efficient surfactants, SDS and Triton X-100, fully displace particles from the interface. They do this by lowering the interfacial tension below that of Pickering emulsions with nanoparticles at the interface. Interfacial energy measurements, surface plasmon and small-angle x-ray spectroscopy are all consistent with this picture.

Less efficient surfactants such as Tween 85 and Span 20 show surprising behavior when mixed with particles. The mixtures lower the interfacial tension more than pure particles and the surfactants do not fully block the interface. A mixture of particles and surfactants apparently forms at the interface that lowers the macroscopic interfacial tension more than each of its components. Similar synergistic effects have been reported for kaolinite clay (with an equivalent spherical diameter of 0.2 μm) at the hexadecane-water interface in the presence of dodecylamine[35] and for the paraffin-water interface in the presence of oleylamine in the oil phase and silica nanoparticles (7 nm diameter) in the aqueous phase.[20]

The synergistic arrangements of particles and surfactants seem kinetically easy to reach. Tween 85 is a polymer (average molecular weight around 1838 g/mol according to the vendor) with a diffusion constant that is at least 1.7 times below that of Span 20, a smaller sorbitan monooleate (molecular weight around 346 g/mol). Both systems rapidly reached stable interfacial tensions in pendant droplets (after 100 s) but not as fast as the system only containing nanoparticles (around 60 s).

The combination of Tween 85 and particles stabilizes the emulsion almost as efficiently as SDS when judged by the droplet size and their evolution. Despite of the relatively low interfacial energy caused by Span 20-particle-combinations, this mixture did not efficiently stabilize emulsions. Resulting emulsions broke when slowly evaporating the oil phase (Figure 2 c), leading to coales-

cence and increase of droplet size. Industrially, Span 20 is used as co-emulsifier together with other surfactants; while particles can play part of this role, their combination did not yield stable emulsions. Tween 85 yielded more stable emulsions, but only SDS provided small droplets that remained small over extended periods of time.

Particle-containing emulsions provide an interesting route to functional particle assemblies: droplets can act as templates that define particle arrangement. The arrangement depends on the distribution of particles in the evaporating droplets. Effective medium theories are simple models that can describe the optical response of small metallic particles in such droplets. Maxwell-Garnett theory assumes randomly distributed (rather than agglomerating or percolating) particles that are much smaller than the wavelength of light in a homogenous medium. It is suitable for the nanoparticles we have here. The theory predicts optical transmission depending on the volume fraction of particles, the value that we observed experimentally. We calculated the surface plasmon peak shift expected for this configuration using Maxwell-Garnett theory [10,25] and compared the predictions to the measured surface plasmon shifts (Figure 2). Emulsions containing Span 20 were too instable to compare to the model but exhibited a continuously increasing shift that suggests a uniform particle distribution in the droplets. For emulsions containing SDS, there is good agreement between predicted and measured shifts. This rules out early agglomeration of the particles and is consistent with SDS blocking the oil-water interface.

Surprisingly, the EMT model also fits the data of Tween 85. We know that AuNP segregate to macroscopic oil-water interfaces in the presence of this surfactant. One may assume that the situation changes for small emulsion droplets and the particles remain in the bulk oil. A more likely explanation of the fit is, however, that the density of nanoparticles at the interface apparently is too low to cause a discernible SPR shift.

It has been theoretically predicted and experimentally demonstrated that the electromagnetic coupling between nanoparticles becomes effective for interparticle distances that are smaller than approximately five times the particle radius ($d < 5R$ where d is the center-to-center distance and R is the radius of the particle).[36,37] For our system, Maxwell-Garnett Theory predicts a surface

plasmon shift below 0.5 nm (our detection limit) for particle distances above 12 nm, which implies a maximum density of 0.39 nanoparticles per square nanometer at the interface of the droplets before discernable shifts occur. We suggest that droplet interfaces stabilized with Tween 85 carry particles at a density below this value.

Small-angle x-ray scattering (SAXS) of shrinking, particle-containing emulsions is dominated by the scattering of AuNP and provides additional structural insights. Time-dependant scattering intensity of our samples showed, for all samples, strong oscillations of the structure factor in the high q region but no oscillations in the low q region. A Pickering phase would cause oscillations in the low q range even for droplets broadly distributed in size. We can rule out such structures. At all times, the evolution of the scattering intensity could be fitted by the cluster model, suggesting particles that are confined but do not form shells.

The hard-sphere clustering model[38] assumes attractive particles and predicts additional scattering $S_c(q)$ when the particles interact and form clusters:

$$S_c(q) = \frac{I_M}{(1+q^2\xi^2)^p}, \tag{4}$$

where I_M is proportional to the average mass of the cluster, is ξ proportional to the characteristic cluster size and p correspond to the fractal dimension. As the solvent from the droplets evaporated, the volume fraction ϕ of nanoparticles increased, the correlation length ξ decreased and the fractal dimension p decreased (see supporting information). The increase in the local volume fraction can be attributed to agglomeration. The correlation length corresponds to the decreasing average droplet sizes during evaporation. The decreasing fractal dimension can be interpreted as sign of increasing confinement and density of the forming supraparticles. The hard-sphere clustering model fits our scattering data and suggests correlation lengths that coincide with the droplet diameters and volume fractions that coincide with particles homogeneously distributed in the available volume (see supporting information).

For the emulsion stabilized by SDS (figure 3 (d)), a SAXS peak appeared around 0.8 nm^{-1}. The

peak shifted to increasing q_c until all dispersed solvent had evaporated. It probably corresponds to the formation of supraparticles with decreasing particle-particle distances similar to the process we previously reported for emulsions stabilzed by Triton X-100.[10] The particle-particle distance d is roughly related to the peaks' positions as $d_c \approx 2\pi q_c$. As the droplets shrink, the particles are compressed to a maximum state, which leads to a peak around $q_c \approx 0.88\,\mathrm{nm}^{-1}$. This peak corresponds to a particle spacing of 7.2 nm, slightly below the value of $d_c \approx 7.7$ nm observed in TEM.

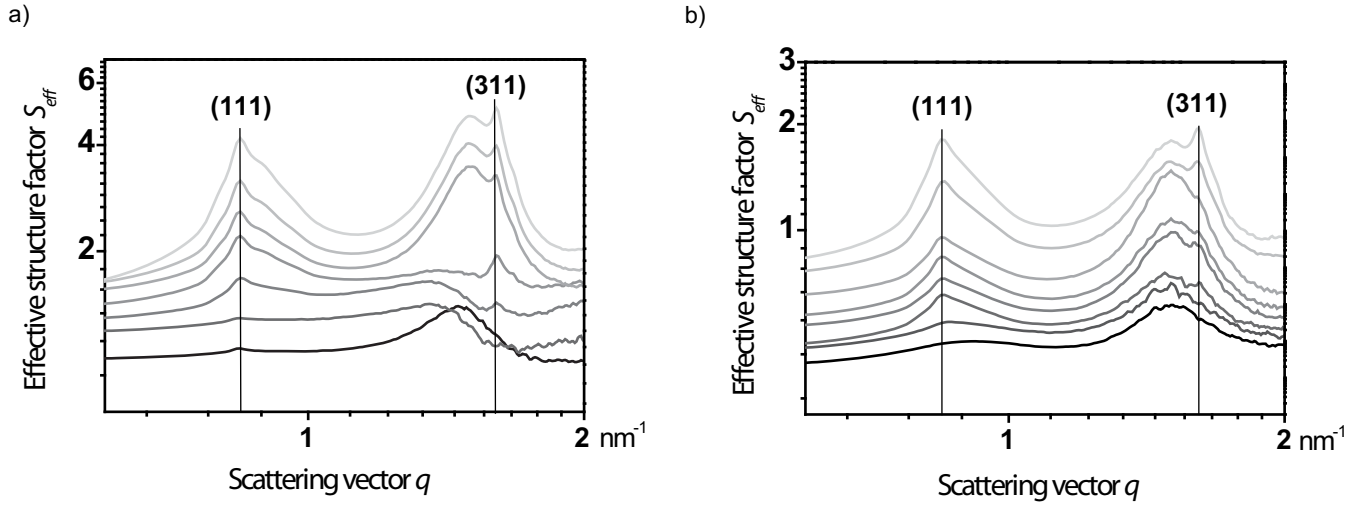

Figure 5: Effective SAXS structure factors of samples containing Tween 85 (a) and Span 20 (b) indicating agglomerates with fcc structure. The maxima are equivalent to Bragg peaks and be can indexed using Bragg's law. They correpospond to (111) and (311) planes with d_{111} spacing of 7.4 nm and d_{311} spacing of 3.9 nm.

For emulsion stabilized by Tween 85 and Span 20, a peak emerged that did not shift upon further evaporation (Figure 3 (d)). We attribute this peak to the formation of agglomerates with constant particle-particle distances. Bragg's law, $q = 2\pi\sqrt{h^2+k^2+l^2}/a$ (where a is the lattice constant and h, k and l are the Miller indices) lets us index the peaks[39] from figure 5 as belonging to (111) and (311) planes for the peak at $q = 0.84\,\mathrm{nm}^{-1}$ and $q = 1.61\,\mathrm{nm}^{-1}$, respectively.

The results so far suggest two different mechanisms of particle arrangement in the droplets that depend on the surfactant: SDS and Triton X-100 keeps particles away from the oil-water interface. Particles are compressed in the oil phase and form structures that are dominated by the free energy

minimization of particle-particle interactions. Tween 85 and Span 20 do not fully exclude particles from the interfaces. The combined interactions between particles at the interface and particles in the oil phase yield agglomerates with fcc packing.

Transmission electron microscopy supports this picture (Figure 4). Particle agglomerates formed in emulsions with SDS remind of icosahedra clusters.[10,40] Tween 85 and Span 20 yield agglomerates having fcc and amorphous structures.

Conclusions

Stability and structure of particle-containing emulsions depend on the choice of surfactant. The extreme cases are "Pickering"-type emulsions that are solely stabilized by particles at the oil-water-interface. At the other extreme, good surfactants such as SDS and Triton X-100 fully block the interface so that all particles remain inside the oil phase.

Intermediate cases are interesting. Both Span 20 and Tween 85 formed mixtures with nanoparticles that efficiently lower the interfacial tension. The resulting emulsions were less stable than that formed with SDS and Triton X-100, but more stable than the Pickering type. Emulsions that only contain alkylthiol-coated AuNP prove too instable to work with.

Manoharan and Pine reported that microparticles adsorbed at oil-water interfaces collapse when the oil phase is evaporated. The spheres form supraparticles with predictable structures.[9,41] We showed previously that nanoparticles arrange into predictable, but structurally different supraparticles when confined to the oil phase of a droplet stabilized by Triton X-100 (or SDS, as we showed here). Although Span 20 and Tween 85 form reasonably stable emulsions in which particles reside at the oil-water interface, the evaporation of the oil phase does not yield any of the structures observed by Manoharan et al. for larger particles. Instead, pieces of fcc crystals form.

Nanoparticles are more mobile than microparticles and dominated by interactions different from those governing microparticles. The smaller particles can find minimum free energy cluster configurations that have not been observed for the larger species. This may also explain why

nanoparticles do not collapse like microparticles when confined at a liquid-liquid interface: where microparticles slowly move, nanoparticles are in constant motion and can fall into local minima of dense fcc packings.

Acknowledgement

The authors thank Michael Sztucki and his colleagues at the ESRF for their support of the SAXS studies and Eduard Arzt for his continuing support of this project. Beam time was granted by the ESRF.

References

(1) Kassiba, A.; Bouclé, J.; Makowska-Janusik, N., M.and Errien *J. Phys.: Conf. Ser.* **2002**, *79*.

(2) Dasgupta, D.; Kamar, Z.; Rochas, C.; Dahmani, M.; Mesini, P.; Guenet, J. M. *Soft Matter* **2010**, *6*, 3573–3581.

(3) Coursault, D.; Grand, J.; Zappone, B.; Ayeb, H.; Lévi, G.; Félidj, N.; Lacaze, E. *Advanced Materials* **2012**, *24*, 1461–1465.

(4) Velev, O.; Furusawa, K.; Nagayama, K. *Langmuir* **1996**, *12*, 2374–2384.

(5) Velev, O.; Furusawa, K.; Nagayama, K. *Langmuir* **1996**, *12*, 2385–2391.

(6) Bai, F.; Wang, D.; Huo, Z.; Chen, W.; Liu, L.; Liang, X.; Chen, C.; Wang, X.; Peng, Q.; Li, Y. *Angewandte Chemie* **2007**, *46*, 6650–6653.

(7) Harrison, R. G.; Washburn, A. L.; Pickett, A. T.; Call, D. M. *J. Mater. Chem.* **2008**, *18*, 3718–3722.

(8) Kim, S.-H.; Cho, Y.-S.; Jeon, S.-J.; Eun, T. H.; Yi, G.-R.; Yang, S.-M. *Advanced Materials* **2008**, *20*, 3268.

(9) Manoharan, V. N.; Elsesser, M. T.; Pine, D. J. *Science* **2003**, *301*, 483–487.

(10) Lacava, J.; Born, P.; Kraus, T. *Nano Letters* **2012**, *12*, 3279–3282.

(11) Bansode, S. S.; Banarjee, S. K.; Gaikwad, D. D.; Jadhav, S. L.; Thorat, R. M. *International Journal of Pharmaceutical Sciences Review and Research* **2010**, *1*.

(12) Cheng, S. Y.; Yuen, C. W. M.; Kan, C. W.; Cheuk, K. K. L. *RJTA* **2008**, *12*.

(13) Mora-Huertas, C.; Fessi, H.; Elaissari, A. *International Journal of Pharmaceutics* **2010**, *385*, 113 – 142.

(14) Pickering, S. U. *J. Chem. Soc., Trans.* **1907**, *91*, 2001–2021.

(15) Binks, B. P.; Rodrigues, J. A.; Frith, W. J. *Langmuir* **2007**, *23*, 3626–3636.

(16) Binks, B. P.; Desforges, A.; Duff, D. G. *Langmuir* **2007**, *23*, 1098–1106.

(17) Ma, H.; Luo, M.; Dai, L. L. *Phys. Chem. Chem. Phys.* **2008**, *10*, 2207–2213.

(18) Whitby, C. P.; Fornasiero, D.; Ralston, J. *Journal of Colloid and Interface Science* **2009**, *329*, 173 – 181.

(19) Vashisth, C.; Whitby, C. P.; Fornasiero, D.; Ralston, J. *Journal of Colloid and Interface Science* **2010**, *349*, 537 – 543.

(20) Eskandar, N. G.; Simovic, S.; Prestidge, C. A. *Journal of Colloid and Interface Science* **2011**, *358*, 217 – 225.

(21) Hait, S. K.; Moulik, S. P. *Journal of Surfactants and Detergents* **2001**, *4*, 303–309.

(22) Wan, L. S. C.; Lee, P. F. S. *Journal of Pharmaceutical Sciences* **1974**, *63*, 136–137.

(23) Ruiz, C. *Colloid and Polymer Science* **1995**, *273*, 1033–1040.

(24) Zheng, N.; Fan, J.; Stucky, G. D. *JACS* **2006**, *128*, 6550–6551.

(25) Garnett, J. C. M. *Philosophical Transactions of the Royal Society of London. Series A, Containing Papers of a Mathematical or Physical Character* **1904**, *203*, 385–420.

(26) Moores, A.; Goettmann, F. *New J. Chem.* **2006**, *30*, 1121–1132.

(27) Novotny, L. *Phys. Rev. Lett.* **2007**, *98*, 266802.

(28) Rakic, A.; Djurišic, A. B.; Elazar, J. M.; Majewski, M. L. *Appl. Opt.* **1998**, *37*, 5271–5283.

(29) Lee, K. S.; El-Sayed, M. A. *J. Phys. Chem. B* **2006**, *110*, 19220–19225.

(30) Sztucki, M.; Narayanan, T. *J. App. Crys.* **2007**, *40*, 459–462.

(31) Glaser, N.; Adams, D. J.; Boeker, A.; Krausch, G. *Langmuir* **2006**, *22*, 5227–5229.

(32) Joos, P.; Vollhardt, D.; Vermeulen, M. *Langmuir* **1990**, *6*, 524–525.

(33) Peltonen, L. J.; Yliruusi, J. *Journal of Colloid and Interface Science* **2000**, *227*, 1 – 6.

(34) Yeung, A.; Dabros, T.; Masliyah, J. *Journal of Colloid and Interface Science* **1998**, *208*, 241 – 247.

(35) Wang, W.; Zhou, Z.; Nandakumar, K.; Xu, Z.; Masliyah, J. H. *Journal of Colloid and Interface Science* **2004**, *274*, 625 – 630.

(36) Ghosh, S. K.; Pal, T. *Chem. Rev.* **2007**, 4797–862.

(37) Barboiu, M. *Constitutional Dynamic Chemistry*; Springer, 2012.

(38) Sztucki, M.; Narayanan, T.; Belina, G.; Moussaid, A.; Pignon, F.; Hoekstra, H. *Phys. Rev. E* **2006**, *74*, 051504.

(39) Korgel, B. A.; Fullam, S.; Connolly, S.; Fitzmaurice, D. *J. Phys. Chem. B* **1998**, *102*, 8379–8388.

(40) Niu, W.; Xu, G. *Nano Today* **2011**, *6*, 265 – 285.

(41) Manoharan, V. N. *Solid State Communications* **2006**, *139*, 557–561.

Graphical TOC Entry